DUPLICATE

Forecasting Development

Forecasting Research Technical Report No. 369

Automatic detection of volcanic ash using Meteosat

By T.R. Scott, K.A. McDonald and R.W. Lunnon

November 2001

© Crown Copyright 2001

Met Office , Forecasting Development , Room R321, London Road , Bracknell , Berkshire ,RG12 2SZ, United Kingdom

00/0486

Forecasting Research
Technical Report No. 369

Automatic detection of volcanic ash using Meteosat

by

T.R. Scott, K.A. McDonald and R.W. Lunnon

November 2001

The Met Office
Forecasting Development
Room R321
London Road
Bracknell
RG12 2SZ
United Kingdom

© Crown Copyright 2001

Permission to quote from this paper should be obtained from the above Met Office division

Please notify us if you change your address or no longer wish to receive these publications.

Tel: 44 (0)1344 856245 Fax: 44 (0)1344 854026 email: jsarmstrong@meto.gov.uk

Automatic detection of volcanic ash using Meteosat

T R Scott, K A McDonald and R W Lunnon

November 2001

Abstract

An automatic volcanic ash detection system has been developed by the Met Office for use by the London VAAC. It searches infrared images from Meteosat for clouds that are near to a volcano and have a shape that might be expected for volcanic ash given the local wind and temperature conditions. With system parameters set to detect 7 test eruptions, the system has detected an eruption of Etna but missed an eruption of Montserrat. The false alarm rate is currently too high for the system to be of operational use. However if the expected cloud shapes can be better defined, and consideration is given to the temporal and spectral characteristics of volcanic ash, then it may be possible to reduce the false alarm rate to a more acceptable level.

1 Introduction

Volcanic ash clouds are a significant hazard to aviation, as they can cause structural damage to an aircraft that is not only costly to repair but can lead to in-flight engine shutdown. Several aircraft have experienced total engine failure following an ash cloud encounter, with the engines only being restarted after significant altitude loss (Casadevall, 1992; Sparks et al., 1997). Similar incidents will continue to occur until timely and accurate information on ash cloud locations is reliably available to the aviation community (Salinas, 1999).

Forecasting the movement of ash that has reached aircraft cruising levels is the responsibility of Volcanic Ash Advisory Centres (VAACs) (Servranckx et al., 1999), but first they need to know that an eruption has occurred. Notification usually comes from eyewitnesses or volcano monitoring centres, but this can be a slow and unreliable process, particularly for volcanos in geographically or politically isolated areas. There is thus a need for a remote sensing system that can automatically detect volcanic ash emissions from volcanos worldwide.

Such a system, based on satellite data, is being developed by the Met Office for intended use by the London VAAC. This paper describes the current state of the system, and considers improvements that could be made to make it fit for operational use.

2 Satellite data

Satellite data suitable for volcanic ash detection by the London VAAC must cover Iceland, their particular area of responsibility. Data from two satellite imaging instruments were considered. One was the Advanced Very High Resolution Radiometer (AVHRR) onboard several of the polar orbiting satellites operated by NOAA. The other was the Visible and Infrared Spin Scan Radiometer (VISSR) onboard Meteosat, a geostationary satellite at 0° longitude operated by EUMETSAT.

AVHRR images available operationally in the Met Office cover Europe and the North Atlantic with five spectral channels having a sub-satellite resolution of 1.1 km. The update interval is irregular and can range from less than half an hour up to 12 hours or more, depending on the number of working instruments and the orbital parameters of their satellites.

VISSR images are full disk images covering the Caribbean, the Atlantic, Europe and Africa. Iceland is at a high latitude and therefore near the edge of the field of view. The images are available in visible, infrared, and water vapour channels, with sub-satellite resolutions of 2.5 km for the visible channel and 5 km for the infrared and water vapour channels. The images are updated every half an hour.

Advantages of the AVHRR images are their higher resolution and greater availability of spectral channels. Multi-spectral imagery can be used to highlight clouds with the spectral characteristics of volcanic ash, as is already automatically done by several VAACs for visual detection and tracking purposes (Streett, 1999; Watkin, 2001). However a big disadvantage of the AVHRR images is their longer update time. For a volcanic ash detection system to be of maximum benefit to aviation it really needs to detect an ash cloud as soon as possible after formation, regardless of the time or location of the eruption.

It was therefore decided to use infrared VISSR images for volcanic ash detection, visible VISSR images being unsuitable because of their unavailability during darkness hours. Although low level volcanic ash may not always be apparent in infrared images, ash reaching aircraft cruising levels should be detectable providing it is unobscured by water or ice cloud. For the rest of this report the VISSR images will be referred to as Meteosat images.

3 Volcanic ash clouds

A volcanic ash detection system based on a single infrared channel must search for clouds having the spatial and temporal characteristics of volcanic ash. Spatial characteristics can include the vertical structure of the cloud top, which is represented in an infrared image by variations in the cloud top brightness temperature.

In an eruption the release of gas pressure can cause hot ash to be propelled into the atmosphere as an eruption column. This column has an initial vertical velocity that decreases rapidly with altitude above the vent due to gravitational deceleration and atmospheric drag from air entrainment. Entrained air is heated by the volcanic ash reducing the density of the column, and if the column becomes buoyant then it continues to rise convectively. Otherwise it falls back to the ground as a pyroclastic flow, which may itself become buoyant and produce eruption columns several kilometers away from the vent (Woods, 1988; Sparks et al., 1997). In satellite images the observed column may thus be offset away from the vent.

A rising eruption column will eventually reach an altitude where it has the same density as the surrounding environment, known as the neutral buoyancy height. From here it will continue to rise under momentum to a maximum height, before falling back to the neutral buoyancy level.

The rise time and maximum height of an eruption column depend on the eruption strength. Strong eruptions can reach altitudes well into the stratosphere within a matter of minutes. They remain undistorted by the wind and spread radially into an umbrella cloud. When viewed from a satellite such a cloud will appear circular until eventually the wind causes it to fan out in the downwind direction. Weaker eruptions can take up to half an hour to reach their maximum altitude somewhere in the middle to upper troposphere. For sustained eruptions the column may be distorted by the wind into a plume spreading downwind from the volcano. For non-sustained eruptions the column

will detach from the volcano and drift downwind, perhaps retaining its original circular shape (Self and Walker, 1994).

The cloud top temperature of an eruption cloud determines the brightness temperature of the cloud as observed in an infrared image. For opaque ash that has settled at the neutral buoyancy height the brightness temperature will approximately equal the ambient air temperature. Ash below the neutral buoyancy height will be warmer than the surrounding air, while that above the neutral buoyancy height will be colder. With time ash will fall out under gravity so cloud top brightness temperature can vary with horizontal distance from the vent (Woods and Self, 1992; Woods et al., 1995). Such temperature structure is unlikely to be resolvable in the low resolution infrared Meteosat images however, particularly for weak eruptions that are only resolved by a small number of pixels.

Assuming an opaque cloud and temperature equalisation, cloud top temperature can be used to calculate cloud top height from a temperature profile of the atmosphere (Sparks et al., 1997). This method gives two solutions, corresponding to a cloud top height either below or above the tropopause.

4 Volcanic ash detection

Volcanic eruptions with maximum heights below and above the tropopause will have different characteristics as observed in infrared images. Therefore two different volcanic ash detection systems are required. Due to limited resources it was decided to concentrate on detecting the more common weak eruptions that do not reach the tropopause. It was also decided that only the spatial characteristics volcanic ash would be considered. These are easier to search for than temporal characteristics because each image can be analysed independently.

Using infrared Meteosat images calibrated to brightness temperatures, the volcanic ash detection system looks for clouds that meet the following conditions.

- *Shape* - the cloud must have a circular shape, or a plume shape spreading downwind.
- *Height* - the cloud top must be at the same height as the wind used for establishing the shape condition.
- *Location* - the cloud top should be within a short distance of a volcano, or downwind of a volcano.
- *Contrast* - the brightness temperature of the cloud must contrast with its immediate surroundings.

The shape, height and location conditions require volcano locations to be specified. Volcanos used in the system have all erupted since 1500AD as listed by the Smithsonian Institute Global Volcanism Program. This cutoff date was chosen to include the majority of historically documented eruptions. The volcanos also have a viewing angle of less than 78°, to include all volcanos in the Caribbean and Iceland, but exclude all those in Central and South America. Figure 1 shows the locations of these volcanos plotted on an infrared Meteosat image.

The implementation of the above conditions will now be described, with reference to an eruption of Hekla in Iceland at 1819Z on 26 February 2000. This eruption produced a plume which rapidly reached an altitude of about 11 km (Hekla eruption, 2000). The plume is shown in figure 2.

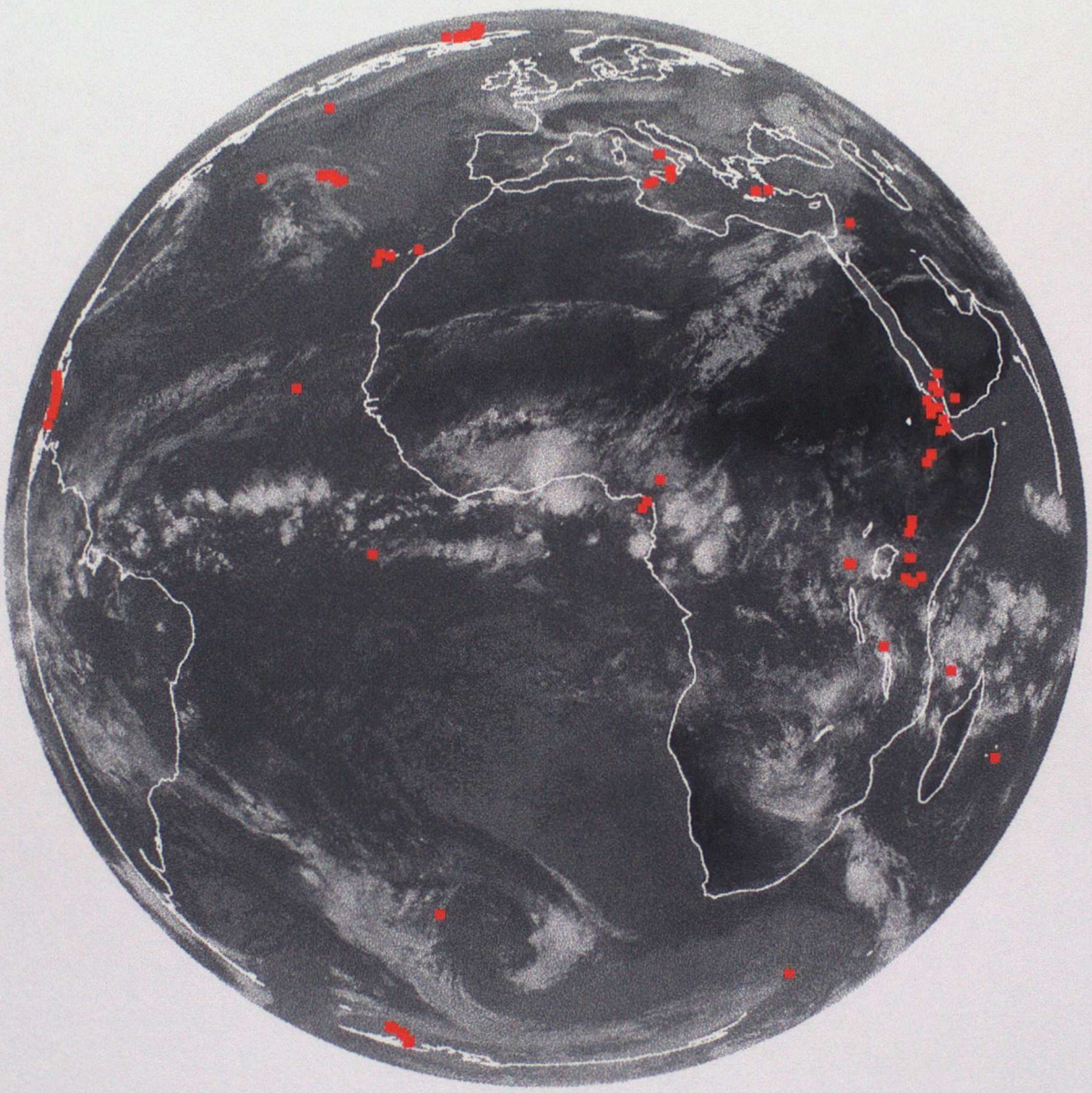

Figure 1: Volcano locations plotted on an infrared Meteosat image, for volcanos that have erupted since 1500AD. The slight discrepancy between the coastlines and the image, as seen at the edges of the image, is due to projection differences.

Figure 2: The eruption plume half an hour into the eruption of Hekla in Iceland on 26 February 2000, as seen in the 1900Z infrared Meteosat image. Brighter pixels correspond to colder brightness temperatures. The location of Hekla is given by the black dot.

4.1 Shape

A cloud is identified as having the correct shape for volcanic ash by checking for a good shape match between the cloud and a cloud that might be expected for volcanic ash. Mathematically this is done by correlating an infrared image with a kernel containing the expected cloud shape. Section 4.1.1 describes how the expected cloud shapes are generated, and section 4.1.2 describes the correlation process.

4.1.1 Expected cloud shapes

A volcanic ash cloud could have either a plume shape or a circle shape, and therefore the infrared images are correlated with kernels representing both of these possible cloud shapes. The kernels are generated as follows.

Plume shape kernels are generated by assuming that a plume emitted by a volcano spreads downwind in a triangular shape with a specified angular width. The volcano is at the centre of the kernel and each pixel in the kernel is assigned a value equal to the fractional coverage of that pixel by the plume. Pixels not covered by the plume, but either horizontally, vertically or diagonally adjacent to at least one pixel covered by the plume, are then assigned the same negative number such that the mean value of the kernel is 0. This offsets the plume against the background and ensures that a neutral correlation result of 0 will be obtained if the kernel is correlated with an image of constant brightness temperature.

The downwind direction is taken to be the wind direction at cloud top height. Cloud shape will probably be most influenced by the wind at this altitude, because it will be of higher velocity than lower altitude winds.

Since the cloud top height is unknown in advance plume shape kernels are generated for each of the 850, 700, 600, 500, 400, 300, 250, 200, and 150 hPa pressure levels. Below 850 hPa ash clouds are almost certainly too warm to be visible in infrared images. Above 150 hPa is approaching the tropopause. The wind directions are taken from preliminary runs of the Met Office's global numerical weather prediction model.

Circle shape kernels are generated in a similar manner, assuming a particular cloud diameter. These kernels do not depend on the wind direction and so are the same for all volcanos and altitudes.

A problem with this method of kernel generation is that it does not account for projection effects in the satellite image. If the angle of view from the satellite to the volcano is large, then the Meteosat instrument will not look directly down on the volcano, so that the observed ash cloud shape will be distorted.

Projection effects could be removed by projecting kernels into the satellite projection, or vice versa, but this has not been implemented. Instead plume shape kernels are generated using not the true wind direction but the wind direction as projected in the satellite image.

Hekla

Using plume-shape kernels of dimension 7×7 with an arbitrary plume angular width of 40°, the best correlation result for the Hekla eruption is obtained for pressure level 300 hPa. This level will therefore be used for demonstrating the detection process.

The wind above the volcano at 300 hPa was forecast by the preliminary midday run of the Met Office's global NWP model with forecast time 1800Z to have westerly and southerly components of 11.8 and 20.0 ms^{-1} respectively. The kernel valid for this wind direction is shown in figure 3, and the projected wind direction and its corresponding kernel are shown in figure 4. Comparison with figure 2 shows that using the projected wind direction improves the alignment of the expected and actual ash clouds.

4.1.2 The correlation

Correlation is commonly used in image processing for shape detection purposes (Gonzalez and Wintz, 1977). It was implemented for volcanic ash detection as follows.

If the image I has dimensions of range $-N_I$ to $+N_I$, and the kernel K has smaller dimensions of range $-N_K$ to $+N_K$, then the correlation result $C_{k,l}$ is given by

$$C_{k,l} = \sum_{i=-N_K}^{+N_K} \sum_{j=-N_K}^{+N_K} \frac{I_{k+i,l+j}}{\iota_{k,l}} \frac{K_{i,j}}{\kappa} \quad \text{for all} \quad -(N_I - N_K) < k, l < +(N_I - N_K). \tag{1}$$

The $\iota_{k,l}$ and κ normalisation factors ensure that $C_{k,l}$ always lies between -1 and 1, such that a perfect match between image and kernel gives $C_{k,l} = 1$. They are calculated using

0.00	0.00	-0.55	0.00	0.92	1.00	0.93
0.00	0.00	-0.55	0.11	1.00	0.83	0.14
0.00	0.00	-0.55	0.31	0.68	0.05	-0.55
0.00	0.00	-0.55	0.12	0.01	-0.55	-0.55
0.00	0.00	-0.55	-0.55	-0.55	-0.55	0.00
0.00	0.00	0.00	0.00	0.00	0.00	0.00
0.00	0.00	0.00	0.00	0.00	0.00	0.00

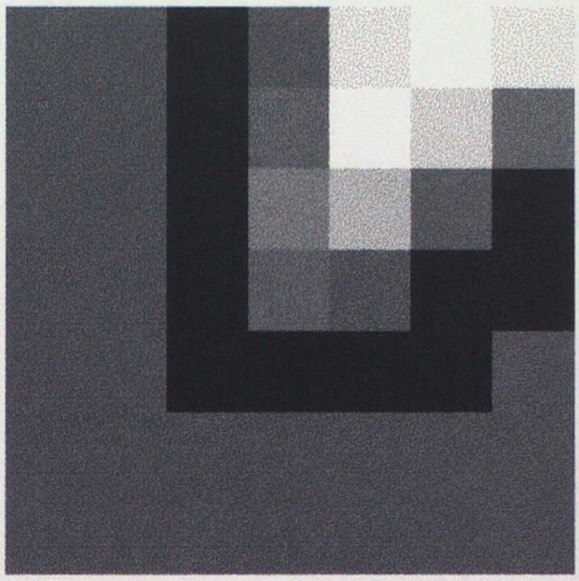

Figure 3: Kernel containing the expected volcanic ash plume at altitude 300 hPa above Hekla, generated using the true wind direction and assuming a plume angular width of 40°. North is upwards and east is to the right. The positive numbers give the fractional coverages of the pixels by the plume. The negative numbers ensure that the mean value of the kernel is zero.

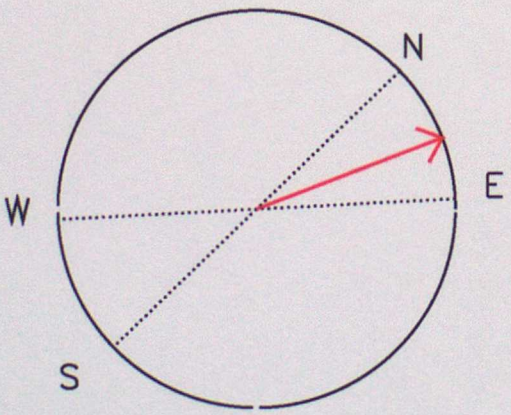

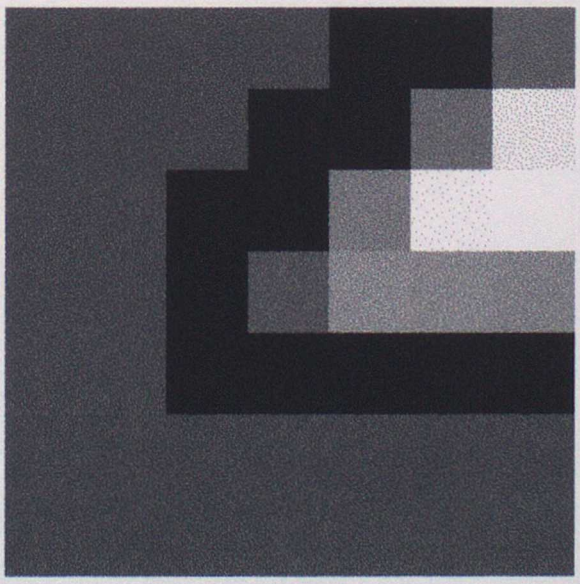

Figure 4: The wind direction at 300 hPa above Hekla in the projection of a Meteosat image, and the corresponding kernel containing the expected volcanic ash plume, generated using the projected wind direction and assuming a plume angular width of 40°.

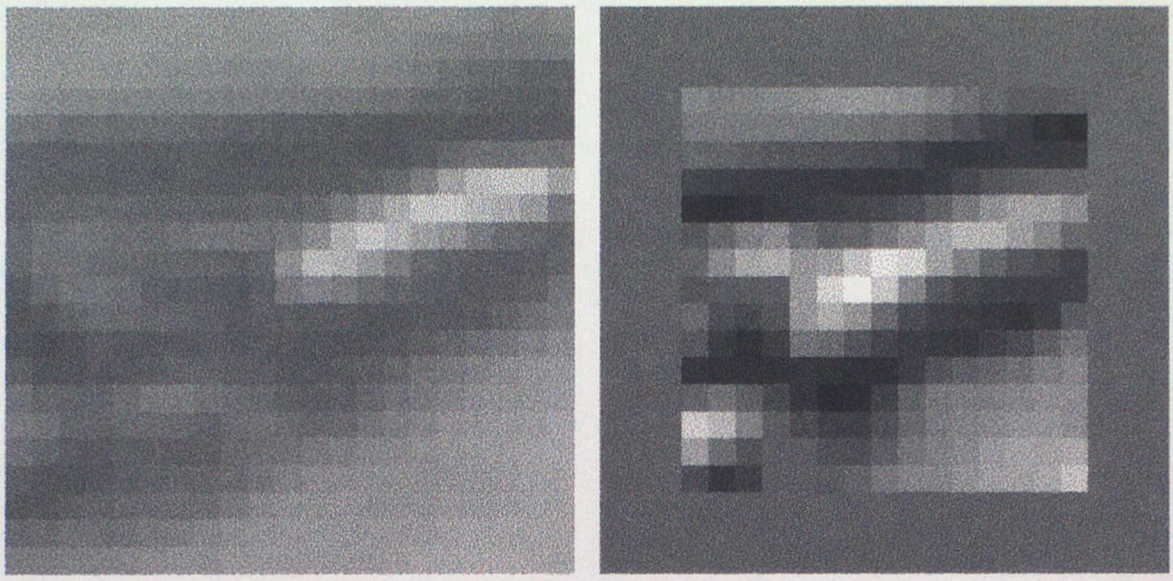

Figure 5: The infrared image $I_{k,l}$ of the Hekla eruption for $N_I = 10$ and the result $C_{k,l}$ of correlating this image with the kernel $K_{k,l}$ shown in figure 4. In both cases the central pixel $(0, 0)$ is directly above the volcano at a height of 300 hPa. The correlation result is scaled black to white from -1 to 1, with lighter colours corresponding to a better match between the image and the kernel. The maximum value is $C_{k,l} = 0.89$ for $k = -1$ and $l = 0$.

$$\iota_{k,l}^2 = \sum_{\substack{i=-N_K \\ \text{for} K_{i,j} \neq 0}}^{+N_K} \sum_{j=-N_K}^{+N_K} (I_{k+i,l+j} - \bar{I}_{k,l})^2 \quad \text{and} \quad \kappa^2 = \sum_{\substack{i=-N_K \\ \text{for} K_{i,j} \neq 0}}^{+N_K} \sum_{j=-N_K}^{+N_K} (K_{i,j} - \bar{K})^2, \tag{2}$$

where

$$\bar{I}_{k,l} = \frac{1}{N} \sum_{\substack{i=-N_K \\ \text{for} K_{i,j} \neq 0}}^{+N_K} \sum_{j=-N_K}^{+N_K} I_{k+i,l+j} \quad \text{and} \quad \bar{K} = \frac{1}{N} \sum_{\substack{i=-N_K \\ \text{for} K_{i,j} \neq 0}}^{+N_K} \sum_{j=-N_K}^{+N_K} K_{i,j}, \tag{3}$$

and N is the number of non-zero pixels contained in the kernel K. The kernel was of course generated in such a way that $\bar{K} = 0$.

Any correlation pixel $C_{k,l}$ that is greater than a pre-defined threshold C gives a positive detection for a volcanic ash shaped cloud.

Hekla

For Hekla, correlating the image with the kernel shown in figure 4 gives the result shown in figure 5. The left hand subfigure is the image and the right hand subfigure is the correlation result. The result shows that there is a good match between the image and the kernel near the volcano, with the highest value being $C_{k,l} = 0.89$ for $k = -1$ and $l = 0$. If this value exceeds the correlation threshold C then the Hekla plume has the correct shape for volcanic ash.

4.2 Height

In establishing the shape condition it is assumed that the volcanic ash has reached a certain pressure level. It is therefore sensible to check that the cloud top height of the detected cloud is actually at this level.

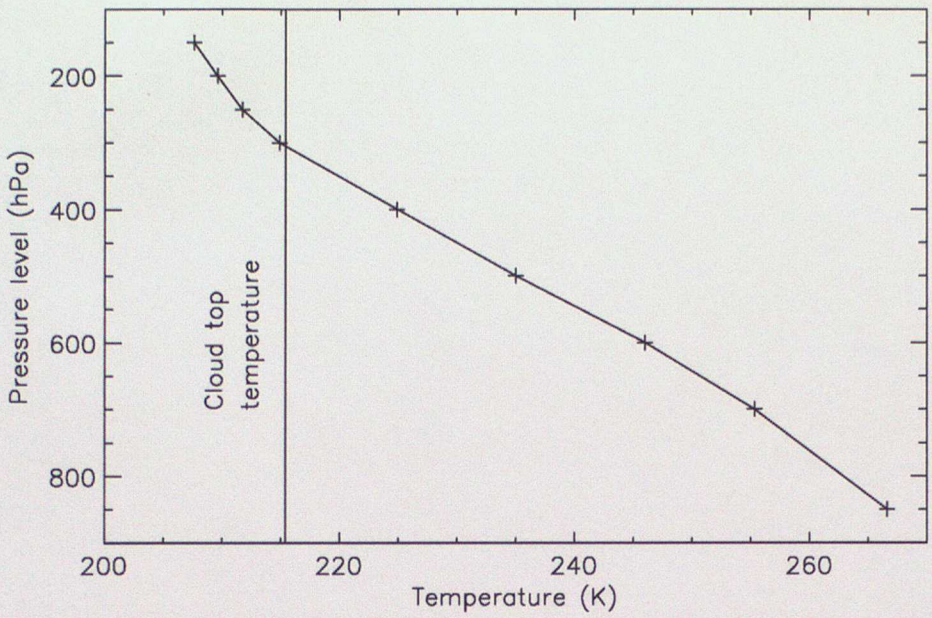

Figure 6: Atmospheric temperature profile above Hekla. The vertical line marks the cloud top temperature of a volcanic ash cloud detected under the assumption that the cloud reached a height of 300 hPa. This figure shows that the detected cloud top is indeed at this height.

The cloud top height is found by comparing the cloud top brightness temperature with a temperature profile of the atmosphere. The cloud top brightness temperature is taken to be the coldest brightness temperature $T_{K,l}$ within the detected cloud, given by

$$T_{k,l} = \text{Min}\Big[I_{k+i,l+j},\ \text{where } K_{i,j} \neq 0 \text{ and } -N_K < i,j < +N_K\Big]. \tag{4}$$

This temperature occurs at the cloud top location $L_{k,l} = (m,n)$. The temperature profile is taken from the Met Office's global NWP model and has values at the 850, 700, 600, 500, 400, 300, 250, 200 and 150 hPa pressure levels. The cloud top height is then the pressure level with temperature closest to the cloud top brightness temperature.

If the cloud top height is not equal to the pressure level used in establishing the shape condition then the cloud is rejected by the detection system. The cloud is also rejected if the cloud top brightness temperature is warmer than the atmosphere at 850 hPa or colder than the atmosphere at 150 hPa.

Hekla

The cloud top brightness temperature for Hekla is $T_{-1,0} = 215.4\,\text{K}$ at location $L_{-1,0} = (1,1)$. From the temperature profile above Hekla shown in figure 6 it can be seen that the profile temperature closest to the cloud top brightness temperature occurs at pressure level 300 hPa. This confirms that the cloud top height is at the correct level for volcanic ash.

4.3 Location

The detected cloud should be in a realistic location relative to the volcano given the local wind speed and direction. The cloud location is taken to be the cloud top location $L_{k,l}$, and this should be either near to the volcano or downwind from the volcano.

The cloud top is considered to be near to the volcano if the distance $R_{k,l}$ between the cloud top and the volcano is less than a threshold distance R. This condition can be expressed mathematically as

$$R_{k,l} = \sqrt{m^2 + n^2} < R. \tag{5}$$

The threshold distance R allows for errors associated with image and kernel pixellation, the fact that lower level winds may have affected the position of the plume, and the fact that the eruption column may have risen from a vent or pyroclastic flow some distance away from the nominal location of the volcano.

Alternatively, the cloud top is considered to be downwind from the volcano if the perpendicular distance $P_{k,l}$ between the cloud top location and the downwind direction is less than the same threshold distance R. If the angular coordinate of the cloud top location is $\theta_{k,l} = \tan^{-1}(n/m)$, and the angular wind direction as it appears in the satellite image is θ, then this condition can be expressed mathematically as

$$|\theta_{k,l} - \theta| < \frac{\pi}{2} \quad \text{and} \quad P_{k,l} = R_{k,l} \sin|\theta_{k,l} - \theta| < R. \tag{6}$$

The cloud top must also be less than a certain time downwind from the volcano, as otherwise the cloud should have been detected in a previous image. This condition is expressed as

$$R_{m,n} < D, \tag{7}$$

where D is the distance between the volcano and a pixel in the satellite image that is a certain time downwind from the volcano.

Hekla

For Hekla the cloud top is at location $L_{-1,0} = (1, 1)$, giving $R_{-1,0} = 1.4$ and $\theta_{-1,0} = 45.0°$. The projected wind direction is $\theta = 21.3°$. Thus $P_{-1,0} = 0.57$. If this value is less than the threshold distance R then the volcanic ash detection remains valid.

4.4 Contrast

The three conditions described above identify all features in an infrared image that have the correct shape, height and location for volcanic ash, even if these features are just minor variations in the cloud top temperature of widespread cloud cover. To overcome this problem, the detection system checks that the detected cloud contrasts significantly against its background.

The contrast between cloud and background is taken to be the brightness temperature variance $S^2_{k,l}$ over the detected cloud. This is given by

$$S^2_{k,l} = \frac{1}{N} \iota^2_{k,l}, \tag{8}$$

where $\iota^2_{k,l}$ and N were defined in equations 2 and 3 respectively. This variance must be greater than a threshold variance S^2 for the detection to be retained.

Hekla

The brightness temperature variance for the detected cloud over Hekla is $S^2_{-1,0} = 135.4$. If this value is greater than the threshold variance S^2 then the detection remains valid.

Eruption	Type	Level	(k, l)	$C_{k,l}$	$T_{k,l}$	$L_{k,l}$	$R_{k,l}$	$P_{k,l}$	D	$S^2_{k,l}$
Nyamuragira	P	500	(-1, 2)	0.83	263	(-3, 2)	3.6	1.4	4.2	46
Montserrat	P	250	(1, -2)	0.94	233	(3, 0)	3.0	2.0	6.9	123
Hekla	P	300	(-1, 0)	0.89	215	(1, 1)	1.4	0.6	20.1	135
Etna 1	C	250	(0, -5)	0.93	225	(0, -5)	5.0	1.7	12.7	435
Etna 2	C	300	(-1, -3)	0.86	242	(-1, -3)	3.2	2.0	13.8	94
Etna 3	P	250	(-2, 0)	0.89	221	(1, 0)	1.0	0.1	9.0	341
Etna 4	P	600	(3, -2)	0.90	278	(6, -3)	6.7	1.4	19.3	28

Table 1: The results of applying volcanic ash detection to the 7 eruptions shown in figure 7. The eruption type specifies whether a plume shape or circle shape cloud was detected. D is the distance 1.5 hours downwind from the volcano in the satellite image.

4.5 Detection parameters

From the preceding section it is obvious that the detection system has a number of free parameters. These can be adjusted to maximise the probability of detection and minimise the false alarm rate.

To gain some idea of the optimal settings, the detection system was tested on the 7 eruptions shown in figure 7. The detection results are given in table 1, for kernels of dimension 7×7 having plume angular widths of 40° or circle diameters of 3.5 pixels. Ideally the latter two parameters should be free to vary, but this was not attempted due to time constraints.

The data for these 7 eruptions were either already available in the Met Office for historical reasons, or were collected in real time during the course of the project as the eruptions occurred. No attempt was made to gather a representative set of eruptions.

From the table it can be seen that parameter settings of

$$C = 0.8, \quad R = 2.5, \quad D = 1.5 \text{ hours}, \quad \text{and} \quad S^2 = 25 \tag{9}$$

allow all of the test eruptions to be detected.

5 Real-time implementation

To demonstrate that the detection system could be used on an operational basis, it was implemented in real-time. Every half an hour the latest infrared Meteosat image received by the Met Office was automatically checked for volcanic ash, using the detection system with parameters set as above in equation 9. A timetable of the events is given in table 2.

The system was run from 6 July 2001 to 9 August 2001 inclusive. During this 35 day period both Etna and Montserrat produced eruption clouds that were visible in infrared Meteosat images. The system detected the Etna eruption, missed the Montserrat eruption, and also produced on average nearly 100 false alarms per day.

5.1 Etna

A major eruption of Etna began on the morning of 17 July 2001. A plume was visible in infrared Meteosat images from about 0700Z on 20 July 2001 until near the end of the eruption on 6 August 2001.

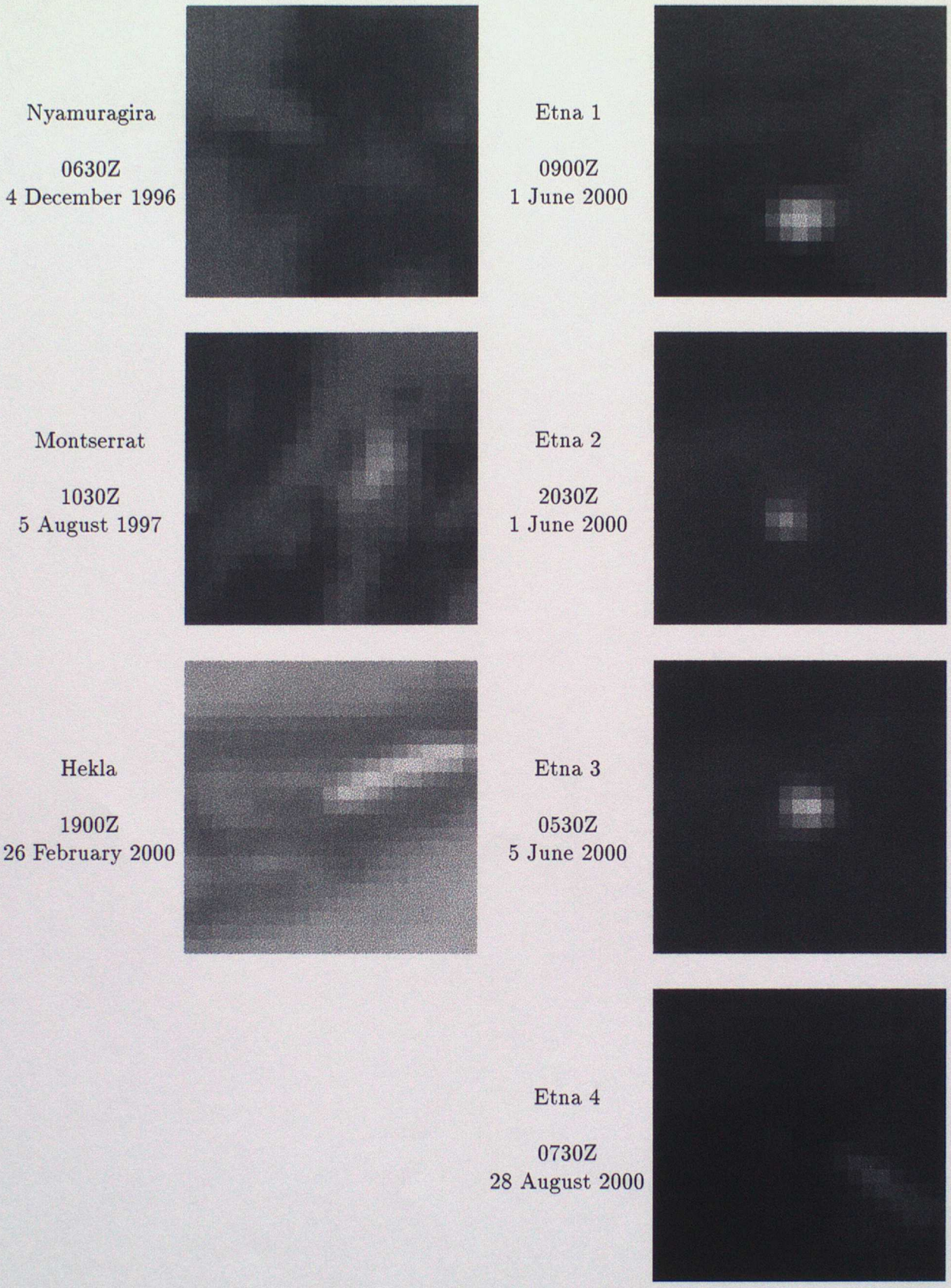

Figure 7: Infrared Meteosat images of the 7 eruptions used for testing the volcanic ash detection system. The images are calibrated to brightness temperatures, and the greyscale runs from 300 K (black) to 200 K (white). For each image the central pixel is the volcano location at detected cloud top height. The Nyamuragira plume extends to the upper left.

Time (am)	Action	Time (pm)	Action
0015	Check 0000 image	1215	Check 1200 image
0045	Check 0030 image	1245	Check 1230 image
0115	Check 0100 image	1315	Check 1300 image
0145	Check 0130 image	1345	Check 1330 image
0205	Update meteorological data (12Z + T15 forecast)	1405	Update meteorological data (00Z + T15 forecast)
0215	Check 0200 image	1415	Check 1400 image
0245	Check 0230 image	1445	Check 1430 image
0315	Check 0300 image	1515	Check 1500 image
0345	Check 0330 image	1545	Check 1530 image
0415	Check 0400 image	1615	Check 1600 image
0445	Check 0430 image	1645	Check 1630 image
0505	Update meteorological data (00Z + T06 forecast)	1705	Update meteorological data (12Z + T06 forecast)
0515	Check 0500 image	1715	Check 1700 image
0545	Check 0530 image	1745	Check 1730 image
0615	Check 0600 image	1815	Check 1800 image
0645	Check 0630 image	1845	Check 1830 image
0715	Check 0700 image	1915	Check 1900 image
0745	Check 0730 image	1945	Check 1930 image
0805	Update meteorological data (00Z + T09 forecast)	2005	Update meteorological data (12Z + T09 forecast)
0815	Check 0800 image	2015	Check 2000 image
0845	Check 0830 image	2045	Check 2030 image
0915	Check 0900 image	2115	Check 2100 image
0945	Check 0930 image	2145	Check 2130 image
1015	Check 1000 image	2215	Check 2200 image
1045	Check 1030 image	2245	Check 2230 image
1105	Update meteorological data (00Z + T12 forecast)	2305	Update meteorological data (12Z + T12 forecast)
1115	Check 1100 image	2315	Check 2300 image
1145	Check 1130 image	2345	Check 2330 image

Table 2: Timetable of events for real-time implementation of the volcanic ash detection system.

In the early stages of the eruption the plume was too low to be detected by the volcanic ash detection system, both because the detection system did not search for ash at a low enough altitude, and because the contrast between the plume and the background was small.

As the eruption progressed the plume strengthened and detections began to occur with increasing frequency. The first detection was at 1330Z on 21 July 2001 for pressure level 850 hPa. The image for this detection is shown in figure 8. The results were $C_{k,l} = 0.82$, $R_{k,l} = 2.8$, $P_{k,l} = 0.2$, $D = 8.5$, and $S^2_{k,l} = 41$. This detection and most of the subsequent detections occurred during the day close to the volcano, when the plume was over land with a warm brightness temperature such that the contrast between the plume and the background was maximised. There were 68 detections in all. Some of these were multiple detections for the same image, with the detected clouds being of different shapes or at different altitudes.

If the detection system had looked for ash as low at 950 hPa, and there had been no contrast condition, then the first detection would have occurred at 0900Z on 20 July 2001 for pressure level 850 hPa. The image for this time is shown in figure 9. Detection results would have been $C_{k,l} = 0.83$, $R_{k,l} = 3.0$, $P_{k,l} = 0.6$, $D = 11.0$, and $S^2_{k,l} = 10$. This detection would have occurred well before the Toulouse VAAC issued their first volcanic ash advisory statement for the eruption at 2000Z on 20 July 2001.

These results suggest that if the volcanic ash detection system was modified to look for ash to low altitudes, and the contrast condition removed, then the system would be capable of detecting ash from fairly low level eruptions. However, this modification would be at the cost of an increased false alarm rate.

5.2 Montserrat

A minor eruption of Montserrat occurred on the morning of 4 August 2001. At 0915Z the Washington VAAC reported the presence of two plumes at altitudes of 4.6 km ($\approx$ 600 hPa) and 9.7 km ($\approx$ 300 hPa).

One of these plumes was visible in the infrared Meteosat images for 0730Z and 0800Z. This was presumably the higher of the two, yet it had a cloud top brightness temperature corresponding to pressure level 500 hPa, which was at an altitude of just 5.9 km. The plume also contrasted poorly against the background.

If the temperature and contrast conditions had been removed from the detection system then the plume would have been detected in the 0730Z image for pressure level 250 hPa, at an altitude of 10.9 km. This altitude corresponds better with the Washington VAAC altitude than does that calculated from the cloud top brightness temperature. The detection results would have been $C_{k,l} = 0.83$, $R = 1.4$, $P = 0.9$, $D = 3.3$ and $S^2_{k,l} = 20$. The image is shown in figure 10.

There are several reasons why the cloud top brightness temperature may give an inaccurate cloud top height, some of which were discussed in section 3. However in this case the large viewing angle from Meteosat to Montserrat was probably a contributing factor. The plume would have been predominantly viewed from the side rather than the top. Furthermore the reduced image resolution makes it likely that the small plume did not completely cover any of the image pixels. Both of these effects would raise the observed brightness temperature, leading to an underestimation of cloud top height.

The detection system may thus perform poorly for eruptions with a large viewing angle, particularly if the eruption cloud is small.

Figure 8: The Etna plume at 1330Z on 21 July 2001. This was the first detection of the plume by the system. The image is calibrated to brightness temperatures, and the greyscale runs from 325 K (black) to 275 K (white). The centre pixel is the volcano location at detected cloud top height.

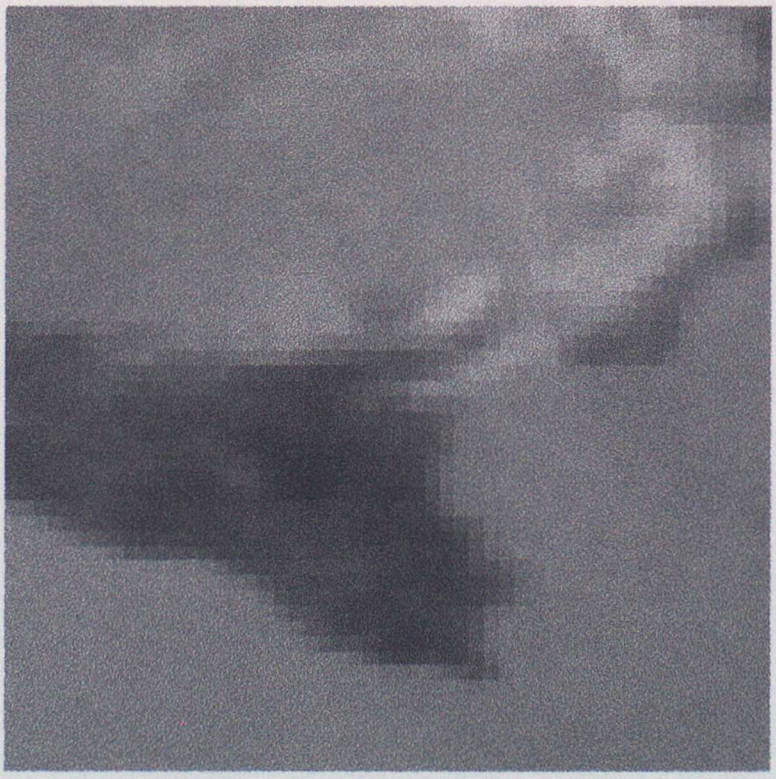

Figure 9: The Etna plume at 0900Z on 20 July 2001. This would have been the first detection of the plume by the system if the system had looked for ash down to an altitude of 950 hPa, and had not had a contrast condition. The image properties are the same as for figure 8.

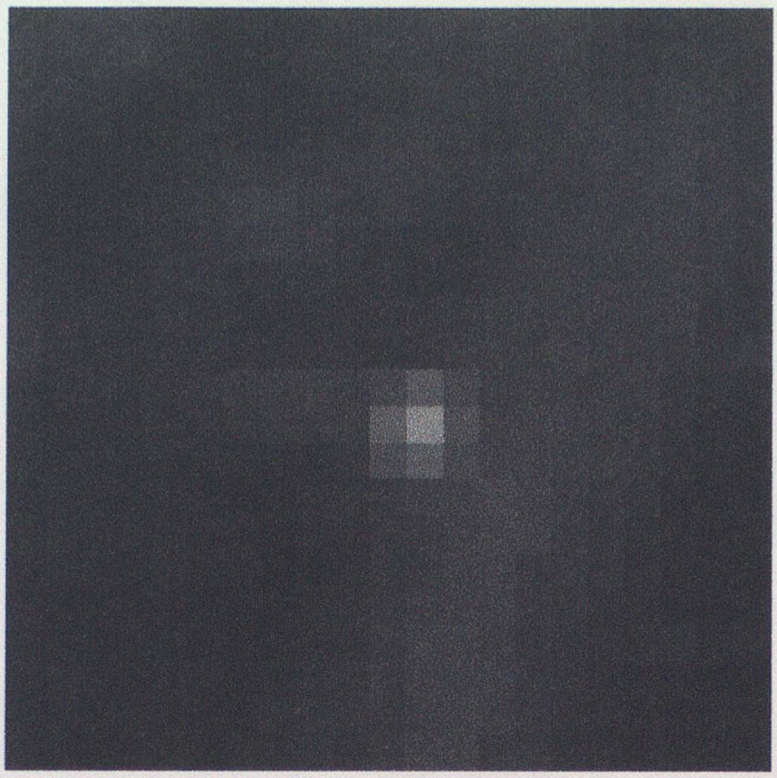

Figure 10: The Montserrat plume at 0730Z on 4 August 2001. This would have been the first detection of the plume by the volcanic ash detection system if the system did not have temperature and contrast conditions. The image is calibrated to brightness temperatures, and the greyscale runs from 300 K (black) to 250 K (white). The central pixel is the volcano location at an altitude of 250 hPa.

5.3 False alarms

During the real-time operation of the detection system there were 3363 false alarms. Given that there were 48 images per day, and 90 volcanos per image, this means that for every examination of a volcano by the detection system there was on average a 2.2% chance of a false alarm. This is a slightly low estimate because not all images were available every day. A better estimate is perhaps 2.4%.

6 Reducing the false alarm rate

The false alarm rate calculated above is too high for the detection system to be of operational use. Several detections per hour would need to be manually verified by the London VAAC, which is about an order of magnitude more than their acceptable rate of a few per day (Smith, 2000). The false alarm rate therefore needs to be reduced. This could be achieved by implementing some of the following options.

- The system parameters could be changed so that the detection conditions are met less frequently. However this option would reduce the detection efficiency for actual eruptions and so is not ideal.

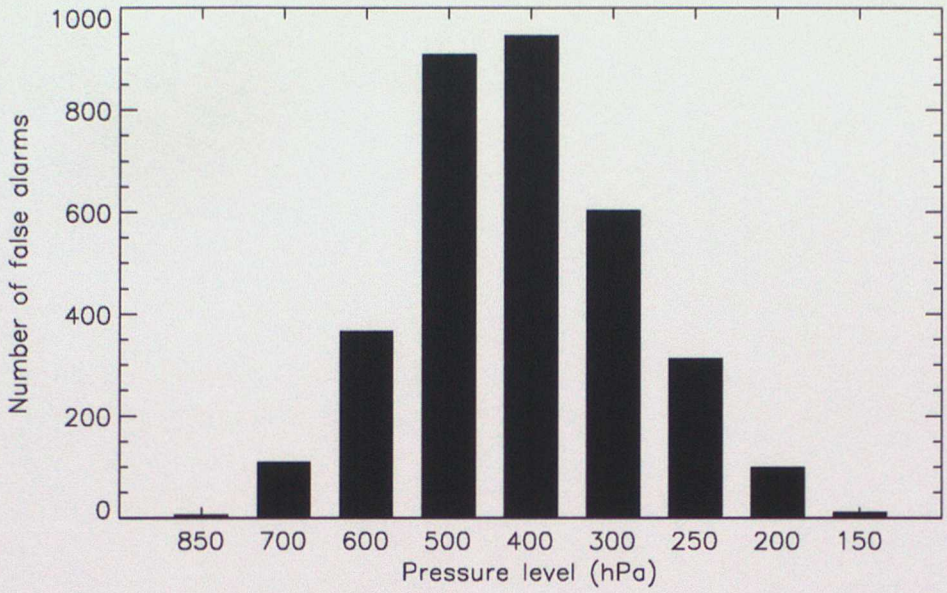

Figure 11: Number of false alarms of the volcanic ash detection system as a function of the pressure level for which the false alarm occurred. The peak in the distribution is to be expected. Low altitude clouds of the correct shape will either fail the contrast condition or be obscured by higher clouds, and high altitude clouds with a small distinct shape are rare.

- The system could monitor only volcanos that are considered as high risk. With just one volcano the false alarm rate would be of the order of 1 per day. However volcanos often erupt without warning and so this option is also not ideal.

- The system could look only for clouds that have reached aircraft cruising levels, such that the cloud top is at a pressure level of 300 hPa or above. This option would more than halve the false alarm rate, as can be seen from figure 11, but would not by itself reduce the rate to an acceptable level.

- The expected cloud shape used in establishing the shape condition could be improved. If the shape could be better modelled, given the atmospheric conditions and an assumed eruption strength, then the correlation threshold C could be raised without reducing detection efficiency. The downwind threshold D could also potentially be reduced by setting it equal to the time taken by the cloud to reach maximum height as determined by the modelling.

- Detection conditions based on temporal information could be included in the system. For example a detected cloud should not be present in a previous image at a location upwind from the volcano. Using a later image to verify the ongoing development of a cloud should not be attempted however, because this would delay the detection process and timeliness would be lost.

- Detection conditions based on spectral information could also be included in the system. The spectral characteristics of the detected cloud should correspond to volcanic ash, not water or ice. It will be possible to include such conditions once multi-spectral infrared images become available from the SEVIRI instrument onboard Meteosat Second Generation (Watkin and Ringer, 2000).

7 Conclusions

This paper has described a volcanic ash detection system designed to provide timely warnings of volcanic eruptions that may compromise aviation safety.

The system uses a shape based method to automatically detect eruption clouds in infrared images from Meteosat, which are updated every half an hour both day and night. A detected cloud has a shape that might be expected for volcanic ash given the local wind and temperature profiles, is either close to or downwind from a volcano, and is reasonably distinct from its surroundings.

System parameters affect the probability of detection and false alarm rate of the system. It has been shown that with the parameters set to detect 7 out of 7 test eruptions the false alarm rate is unacceptably high. Changing the parameters to give an acceptable false alarm rate would make the probability of detection too low. The detection system is therefore unsuitable for its purpose in its current form.

However, use of a shape based approach for volcanic ash detection seems promising. An eruption of Etna was successfully detected, and if a few simple changes had been made to the system then the detection would have occurred before the first volcanic ash advisory statement was issued. Although an eruption of Montserrat was missed this was probably because the eruption was small and near the edge of the field of view. If the detection method had been applied to an image with a smaller angle of view then the eruption may well have been detected.

It thus seems worthwhile to put further effort into improving the shape based detection method. There is considerable scope for this, from better modelling of the expected ash cloud, to the use of temporal and spectral information. Should this work prove successful then the method could become a valuable tool for supporting the work of the VAACs.

A Acronyms

AVHRR	Advanced Very High Resolution Radiometer
EUMETSAT	European Organisation for the Exploitation of Meteorological Satellites
NOAA	National Oceanic and Atmospheric Administration
SEVIRI	Spinning Enhanced Visible and Infrared Imager
VAAC	Volcanic Ash Advisory Centre
VISSR	Visible and Infrared Spin Scan Radiometer

References

Casadevall, T. J. (1992). Volcanic hazards and aviation safety: lessons of the past decade. *FAA Aviation Safety Journal*, 2(3):9–17.

Gonzalez, R. C. and Wintz, P. (1977). *Digital Image Processing.* Addison-Wesley.

Hekla eruption (2000). *Bulletin of the Global Volcanism Network*, 25(02). http://www.volcano.si.edu/gvp/volcano/region17/ice_s/hekla/var.htm.

Salinas, L. J. (1999). Volcanic ash clouds pose a real threat to aircraft safety. In *Eighth Conference on Aviation, Range, and Aerospace Meteorology*, pages 322–325. Amer. Meteorol. Soc.

Self, S. and Walker, G. P. L. (1994). Ash clouds: characteristics of eruption columns. In Casadevall, T. J., editor, *Volcanic Ash and Aviation Safety: Proceedings of the First International Symposium on Volcanic Ash and Aviation Safety*, U.S. Geological Survey Bulletin 2047, pages 65–74.

Servranckx, R., Chen, P., and Little, K. (1999). Volcanic Ash Advisory Centres - roles and challenges. In *Eighth Conference on Aviation, Range, and Aerospace Meteorology*, pages 253–256. Amer. Meteorol. Soc.

Smith, D. (2000). Private communication.

Sparks, R. S. J., Bursik, M. I., Carey, S. N., Gilbert, J. S., Glaze, L. S., Sigurdsson, H., and Woods, A. W. (1997). *Volcanic Plumes*. Wiley.

Streett, D. (1999). Satellite-based volcanic ash advisories and an ash trajectory model from the Washington VAAC. In *Eighth Conference on Aviation, Range, and Aerospace Meteorology*, pages 290–294. Amer. Meteorol. Soc.

Watkin, S. (2001). A description of an AVHRR volcanic ash detection product and examples of its application. Forecasting Research Technical Report 358, Met Office.

Watkin, S. and Ringer, M. A. (2000). Investigation into the use of SEVIRI imagery for the automatic detection of volcanic ash clouds. Forecasting Research Technical Report 297, Met Office.

Woods, A. W. (1988). The dynamics and thermodynamics of eruption columns. *Bull. Volcanol.*, 50:169–191.

Woods, A. W., Holasek, R. E., and Self, S. (1995). Wind-driven dispersal of volcanic ash plumes and its control on the thermal structure of the plume top. *Bull. Volcanol.*, 57:283–292.

Woods, A. W. and Self, S. (1992). Thermal disequilibrium at the top of volcanic clouds and its effects on estimates of cloud height. *Nature*, 355:628–630.